

Robustness of vorticity in electron fluids

Khachatur G. Nazaryan^a, Leonid Levitov^b

^a*Moscow Institute of Physics and Technology, Dolgoprudny, Moscow Region, Russia and*

^b*Department of Physics, Massachusetts Institute of Technology, Cambridge, MA 02139*

(Dated: March 13, 2022)

Electron fluids have been predicted to display flow patterns featuring macroscopic vortices. While this behavior attracted interest as a signature of electron viscosity, linking it to the underlying mechanisms of carrier interaction and scattering on a microscale has remained an outstanding problem. We demonstrate that vorticity is linked to nonlocal conductivity response, no matter what origin. This makes vorticity a robust property transcending the boundaries of the hydrodynamic phase and being significant also in the ballistic phase. Vorticity values, evaluated in a simple geometry, are found to be similar in both phases. However, vortices in viscous electron fluids are orders-of-magnitude more sensitive to the presence of disorder than in the ballistic phase. The effect of disorder therefore provides a clear diagnostic of the microscopic origin of vorticity in electron systems.

Spatial patterns of currents in conductors, observable on macroscales, encode information about carrier dynamics and interactions on microscales[1–8]. Recently, vortices in hydrodynamic electron flows attracted interest as a striking testable signature of microscopic physics in these systems [9–12]. In the studies of electron fluids it is often taken for granted that vorticity, manifested through currents flowing against externally applied electric fields, is a signature of electron viscosity. Here, we discuss conditions under which vortex patterns in electron fluids can occur, focusing on laminar flows describing the regime of low currents relevant for the ongoing experimental work [13–16].

We find that vortices, rather than being unambiguously associated with viscous flows, are a generic attribute of systems with dispersive (k -dependent) conductivity that describes a nonlocal current-field response, see Eqs.(1), (2). We illustrate this behavior by a detailed comparison of vortex flows in different regimes in a simple strip geometry pictured in Fig.1, with carriers injected and drained through a pair of contacts positioned at the opposite sides of the strip. Tuning the system from the viscous regime, occurring at a high electron-electron collision rate, to the ballistic free-electron regime, we find that the vorticity does not disappear when the electron collision rate decreases. To the contrary, overall the vorticity experiences little change upon the viscous-to-ballistic crossover, taking similar values in the ballistic and viscous regimes.

The robustness and generic character of vorticity in electron flows prompts a question of whether the vortex patterns observed experimentally can be unambiguously linked to the microscopic interactions and scattering mechanisms. Naively, judging from Fig.1 this may seem challenging. Indeed, despite vortex flows patterns have somewhat different structure in the viscous and ballistic regimes, they feature comparable vorticity values. However, while vorticity experiences little change upon the viscous-to-ballistic crossover, its dependence on momentum-relaxing collisions is completely different in the two cases. Vorticity is suppressed by momentum re-

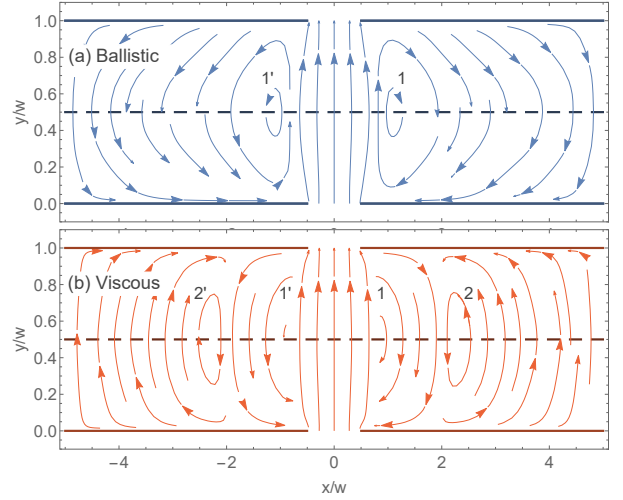


FIG. 1. Vortices in a laminar (linear response) regime in ballistic (a) and viscous (b) flows in a strip geometry. Current enters the strip through a slit on one side and exits through a slit on the opposite side. Parameters used: $\gamma = 0.1 v/w$ in (a), $\gamma = 100 v/w$ in (b), the slit width equal to the strip width (see text). The two flows feature vortices of comparable intensity but different structure: two pairs of vortices in the viscous regime at $x_{1,1'} \approx \pm w$ and $x_{2,2'} \approx \pm 2w$ vs. one pair in the ballistic regime. The interpolated current distributions used to picture the flows, while accurately representing the flow geometry, misrepresent the vorticity magnitude. The latter is quantified by the stream functions shown in Fig.2, indicating that vorticity values are quite similar in the two regimes.

laxation, with the suppression being orders-of-magnitude stronger in the viscous regime than in the ballistic regime. As we will see, a minuscule momentum relaxing scattering is sufficient to suppress the vorticity of viscous flows, leaving vorticity of ballistic flows practically unchanged. The dependence on momentum-relaxing collisions can therefore serve as a diagnostic allowing to delineate between ballistic and viscous vortices.

The resilience of macroscopic vorticity to disorder in the viscous regime and its comparatively abrupt suppres-

sion in the ballistic regime can be understood from the structure of the dispersive conductivity describing the nonlocal current-field response

$$j_\alpha(\mathbf{x}) = \int d^2x' \sigma_{\alpha\beta}(\mathbf{x} - \mathbf{x}') E_\beta(\mathbf{x}'). \quad (1)$$

As it will soon be clear, the momentum dispersion of conductivity is the key property responsible for the formation of vortices. Namely, vorticity of the flow reflects the k dependence of conductivity no matter what origin, ballistic, viscous, or else:

$$j_\alpha(\mathbf{k}) = \sigma_{\alpha\beta}(\mathbf{k}) E_\beta(\mathbf{k}), \quad \sigma_{\alpha\beta}(\mathbf{k}) = \int d^2x e^{-i\mathbf{k}\mathbf{x}} \sigma_{\alpha\beta}(\mathbf{x}). \quad (2)$$

At the same time, a k -independent conductivity describes ohmic transport with a local current-field relation; in this case the flow is potential and vortex-free. Therefore, the threshold for vorticity suppression by disorder can be inferred directly from the conductivity k dependence.

We illustrate this behavior using dispersive conductivity obtained from a simple model (see below):

$$\text{a) } \sigma_{\text{ball}}(\mathbf{k}) = \frac{D}{\gamma_0 + \nu|\mathbf{k}|/2}; \quad \text{b) } \sigma_{\text{visc}}(\mathbf{k}) = \frac{D}{\gamma_0 + \nu\mathbf{k}^2} \quad (3)$$

with $D = ne^2/m$ the Drude spectral weight and $\nu = v^2/4\gamma$ the kinematic viscosity. Here γ_0 is the momentum relaxation rate due to disorder, γ is the electron-electron collision rate that governs viscosity, and in the viscous case the long wavelength limit $kv \ll \gamma$ is assumed. The quantity in the denominators is the disorder scattering rate γ_0 corrected by a k -dependent contribution describing momentum relaxation due to momentum spreading over the lengthscales $\ell \sim 1/k$. The k values for which this contribution becomes smaller than γ_0 define the lengthscales beyond which the conductivity is effectively local, yielding a current flow that is potential and vortex-free.

For transport in a system of size w the relevant wavenumber values, describing momentum escaping from the systems, are $k \sim 1/w$. Comparing to Eq.(3), this predicts the threshold values for disorder scattering above which the momentum dependence of conductivity is suppressed, respectively for the ballistic and viscous regimes:

$$\text{a) } \gamma'_0 \approx \nu/w; \quad \text{b) } \gamma''_0 \approx \nu/w^2 \quad (4)$$

Condition a) states that vorticity is suppressed when the disorder mean free path is smaller than the system size. Condition b) states that the momentum relaxation time is shorter than the time momentum diffuses across viscous fluid in a system of size w , which is a considerably more stringent condition than a). These two threshold values are related as

$$\gamma''_0/\gamma'_0 \approx \ell_{ee}/w \quad (5)$$

where $\ell_{ee} = v/\gamma$ is the el-el collision mean free path. We see that in a hydrodynamic regime, $\ell_{ee} \ll w$, the

sensitivity of vortices to momentum-relaxing collisions is orders of magnitude stronger than in the ballistic regime.

Our geometry of interest is an infinite strip of width w , $-\infty < x < \infty$, $0 < y < w$, with a pair of slits on opposite sides serving as the injector and drain contacts, Fig.1. In this geometry, we will solve for the current distribution for a general nonlocal current-field linear response relation given in Eq.(1). We adopt no-slip boundary conditions modeled using a fictitious field $\mathbf{E}^{(fic)}$ concentrated at the boundary, as discussed below. The distribution of the electric field $\mathbf{E}(\mathbf{x})$ that drives the current, and that of the fictitious field $\mathbf{E}^{(fic)}(\mathbf{x})$ will be determined from the solution of the transport problem within the strip.

To prepare for the discussion of nonlocal transport in a strip, we first consider the properties of the k -dependent conductivity, Eq.(2), found by Fourier transforming the translation-invariant linear response function in Eq.(1). In general, the conductivity $\sigma_{\alpha\beta}(\mathbf{k})$ takes different values for fields and currents parallel and perpendicular to the wavevector \mathbf{k} , such that

$$j_\perp(k) = \sigma_\perp(k) E_\perp(k), \quad j_\parallel(k) = \sigma_\parallel(k) (E_\parallel(k) - i\mathbf{k}\delta\mu(k)) \quad (6)$$

where we added a term $\delta\mu(\mathbf{k})$ to describe the potential of a space charge that builds up due to the spatial nonuniformity of current. In a steady state described by a time-independent field and current, the potential $\delta\mu(\mathbf{x})$, determined from the continuity relation $\text{div}\mathbf{j} = 0$, cancels the longitudinal component E_\parallel . Namely, for a time-independent field and current there is no longitudinal current $\mathbf{j}\parallel\mathbf{k}$ because of charge continuity. As a result, transport is described solely by $\sigma_\perp(\mathbf{k})$ through a relation between transverse components of \mathbf{j} and \mathbf{E} given by a \mathbf{k} -dependent conductivity:

$$\sigma_{\alpha\beta}(\mathbf{k}) = \sigma(k) \left(\delta_{\alpha\beta} - \hat{\mathbf{k}}_\alpha \hat{\mathbf{k}}_\beta \right). \quad (7)$$

From now on, for conciseness, we drop the subscript \perp .

The quantity $\sigma(k)$ can be found from the transport equation for quasiparticles at the Fermi surface. A direct analysis, described in Supplement, gives

$$\sigma(k) = \frac{D}{\gamma_0 + \Gamma(k)}, \quad \Gamma(k) = \frac{z}{\gamma_1 + \frac{z}{\gamma_2 + \frac{z}{\gamma_3 + \dots}}} \quad (8)$$

where $D = ne^2/m$, $z = k^2v^2/4$, and the quantities γ_m are the eigenvalues of the linearized collision operator describing the relaxation rates for different harmonics of particle distribution, $\delta f_\theta(\mathbf{x}, t) = e^{i\mathbf{k}\mathbf{x} - i\omega t} \sum_m e^{-\gamma_m t} \delta f_m e^{im\theta}$, where θ is the azimuthal angle on the Fermi surface.

This general form of $\sigma(k)$ describes a variety of different regimes of interest. The rate γ_0 describes momentum relaxation due to disorder or phonon scattering, the quantity $\Gamma(k)$ describes relaxation of momentum by particles transporting it away from the region of interest. Here, for simplicity, we consider the case of equal rates,

$\gamma_1 = \gamma_2 = \dots \equiv \gamma$, sufficient for exploring vorticity in the viscous, ballistic and ohmic regimes, as well as in the crossover between these regimes. In this case, the quantity $\Gamma(k)$ is readily evaluated, giving

$$\Gamma(k) = \frac{-\gamma + \sqrt{\gamma^2 + k^2 v^2}}{2}. \quad (9)$$

The k -dependent conductivity $\sigma(k)$ defines a scale-dependent linear response. At small k (large lengthscales) such that $\Gamma(k) < \gamma_0$ it describes ohmic dissipation due to disorder scattering. At large k (small lengthscales) such that $\Gamma(k) > \gamma_0$ it describes momentum dissipation due to particle transport within the system. The large- k behavior can be either ballistic or fluid-like, depending on the ratio of γ and kv . Namely, for $\gamma \ll kv$ we have $\Gamma(k) = |k|v/2$, giving an expression in Eq.(3) a), whereas for $\gamma \gg kv$ we have $\Gamma(k) = k^2 v^2 / 4\gamma$, giving an expression in Eq.(3) b).

For transport in a strip of width w the characteristic wavenumber is $k \approx 1/w$. Accordingly, in our simulation we will use $\gamma = 0.1v/w$ and $100v/w$ to model the ballistic and hydrodynamic regimes, respectively; the values $\gamma = 1v/w$ and $10v/w$ will be used for modeling the crossover from between these regimes.

Next we discuss the strategy for tackling the nonlocal transport problem in a strip. This problem will be dealt with by replacing the strip geometry with an infinite 2D plane geometry and, simultaneously, introducing suitable boundary conditions to make the infinite-space problem mimic that for the finite-width strip. Passing to the infinite-space setting allows to fully benefit from the translation invariance of the current-field relation, Eq.(1). The latter then becomes an exact property and can be conveniently handled in a Fourier representation.

To solve the boundary-value problem in the infinite-space representation, we use the linear response relation, Eq.(1), with an electric field corrected by a fictitious electric field of value chosen to null the current at the boundary:

$$E_\beta(\mathbf{x}) = E_\beta^{(ext)}(\mathbf{x}) - E_\beta^{(fic)}(\mathbf{x}), \quad E_\beta^{(fic)}(\mathbf{x}') = \lambda j_\beta(\mathbf{x}') \quad (10)$$

where the fictitious field $E_\beta^{(fic)}(\mathbf{x})$ is defined at system boundary through a relation with the current at the boundary, with λ a ‘boundary resistivity’ parameter (see [17, 18]). We will derive and solve equations that are valid for any λ . Then, in the numerical analysis of the

results we will take a large enough value for this parameter ($\lambda = 10^5 v$) to simulate non-slip boundary conditions. The field $E_\beta^{(ext)}$ is a constant external field along the y axis, it can be integrated over, leaving an additive term $j_\alpha^{(ext)} = j_0 \delta_{\alpha,y}$, which is the current that we inject into our system.

It is convenient, for the purpose of analysis, to rewrite the current-field relations with the fictitious boundary fields, Eq.(10), by introducing a window function for the slit $\chi(x) = 1$ for $|x| \geq w/2$, and 0 for $|x| < w/2$. the current-field Eq.(1) Since the fictitious field exists only at the strip boundaries $y = 0$ and w , Eqs.(1) and (10), relate currents in the strip bulk and currents at the boundaries:

$$j_\alpha(\mathbf{x}) = j_0 \delta_{\alpha,y} - \lambda \int d\mathbf{x}' \delta(y') \chi(x') \sigma_{\alpha\beta}(\mathbf{x} - \mathbf{x}') j_\beta(\mathbf{x}') + \\ - \lambda \int d\mathbf{x}' \delta(y' - w) \chi(x') \sigma_{\alpha\beta}(\mathbf{x} - \mathbf{x}') j_\beta(\mathbf{x}') \quad (11)$$

The symmetry of the strip with a pair of slits imposes the relations for the components of the current,

$$j_y(y, x) = j_y(y, -x); \quad j_y(y, x) = j_y(w - y, x) \quad (12)$$

$$j_x(y, x) = -j_x(y, -x); \quad j_x(y, x) = -j_x(w - y, x) \quad (13)$$

Eqs.(11) for these quantities can be Fourier-transformed to obtain integral equations for the Fourier harmonics of currents at the boundaries $j_\alpha(x, y) = \int \frac{dq}{2\pi} j_\alpha(q, y) e^{-iqx}$:

$$j_y(q, y) = 2\pi j_0 \delta(q) - \lambda \Sigma_{yy}(q) (\tilde{\chi}(q) * j_y(q, 0)) \\ + i\lambda \Sigma_{yx}(q) (\tilde{\chi}(q) * j_x(q, 0)) \quad (14)$$

$$j_x(q, y) = -\lambda \Sigma_{xx}(q) (\tilde{\chi}(q) * j_x(q, 0)) \\ + i\lambda \Sigma_{xy}(q) (\tilde{\chi}(q) * j_y(q, 0)) \quad (15)$$

(for the derivation, see Supporting Materials I). Here we used the symmetry relations for current components at $y = 0$ and w to eliminate the $y = w$ quantities in favor of the $y = 0$ quantities. We also introduced Fourier harmonics of the slit window function $\tilde{\chi}(q) = \int dx \chi(x) e^{iqx} = 2\pi \left(\delta(q) - \frac{1}{\pi} \frac{\sin(qw)}{q} \right)$. The notation $*$ stands for the convolution $(\tilde{\chi}(q) * j_\alpha(q, 0)) = \int_{-\infty}^{\infty} \tilde{\chi}(q - q') j_\alpha(q', 0) dq'$, and the quantities $\Sigma_{i'i'}$ (q) are defined as

$$\Sigma_{yy}(q) = \int \frac{dk_y}{2\pi} [\cos(k_y y) + \cos(k_y (w - y))] \frac{\sigma(\kappa) q^2}{\kappa^2}; \quad \Sigma_{yx}(q) = \int \frac{dk_y}{2\pi} [\sin(k_y y) + \sin(k_y (w - y))] \frac{\sigma(\kappa) q k_y}{\kappa^2} \quad (16)$$

$$\Sigma_{xx}(q) = \int \frac{dk_y}{2\pi} [\cos(k_y y) - \cos(k_y (w - y))] \frac{\sigma(\kappa) k_y^2}{\kappa^2}; \quad \Sigma_{xy}(q) = \int \frac{dk_y}{2\pi} [\sin(k_y y) - \sin(k_y (w - y))] \frac{\sigma(\kappa) q k_y}{\kappa^2} \quad (17)$$

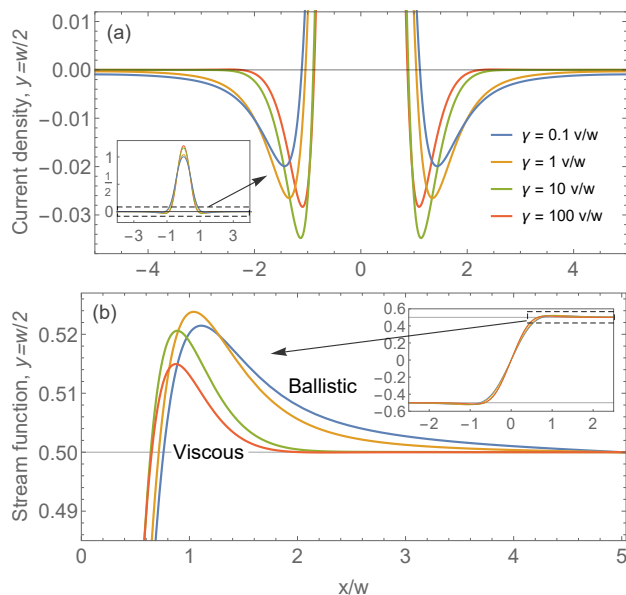


FIG. 2. (a) Current backflow in the viscous, ballistic and intermediate regimes on the line $y = w/2$ in the middle of the strip. The backflow magnitude is nearly the same in all regimes, being slightly larger in the intermediate regime than in the viscous and ballistic regimes. (b) Stream function $\phi_{y=w/2}(x)$ normalized as $\phi_{y=w/2}(x)|_{-L/2}^{L/2} = 1$ for different regimes, detailing the backflows. The largest magnitude is for $\gamma = 1v/w$ (intermediate regime). The inset shows the full stream function.

where we introduced notation $\kappa^2 = q^2 + k_y^2$.

The right-hand side in Eqs.(14) and (15) contains only the currents on the lower boundary $y = 0$. We therefore set $y = 0$ to obtain a pair of coupled linear integral equations for $j_x(q, 0)$ and $j_y(q, 0)$. Because of the convolution these integral equations cannot be solved analytically, therefore a numerical approach must be used. For this we introduce an interval $-L/2 < x < L/2$ on the x -axis, discretized with a mesh of spacing L/N with a large enough N . For the functions in this interval we assume periodic boundary conditions. In Fourier representation, these functions are sums of harmonics with a discrete set of wavenumbers chosen as $q_i = (i - \frac{N-1}{2}) \Delta q'$, $i = 1, 2, \dots, N$ with a step size $\Delta q' = 2\pi/L$. We solve our equations on this dual lattice, approximating integrals as Riemann sums. An inverse Fourier transform is then carried out to find the currents in interval $-L/2 < x < L/2$ in real space. Thanks to the discretization the convolution in each Eqs.(14),(15) yields a linear operator representing the corresponding integral by a $N \times N$ matrix. This allows us to solve the resulting linear equations by inverting matrices.

We first consider the results for the disorder-free case ($\gamma_0 = 0$ in (8)). After solving for currents at $y = 0$ as described above, we use (14), (15) to find currents in the strip bulk. Below we discuss the behavior on a line in the middle of the strip $y = w/2$. The resulting current profile, pictured in Fig.2(a) shows that on both sides of

the direct current flowing from injector to drain there are regions where current flows against the applied field, signaling the presence of vortices. Vortices are seen to be present in both the ballistic and viscous regime. Notably, the vortices have similar intensities in the two regimes, with a little change at the crossover.

One difference between vortices in the two regimes is in their spatial extent: ballistic vortices are about ~ 2 times wider than viscous vortices. Another (minor) difference is that current undergoes multiple sign reversals, indicating the presence of several vortices of opposite orientation (so-called Moffatt vortices[20, 21]). This confirms the presence of multiple vortices in the viscous regime, in line with the flow pictured in Fig.1. However, Fig.2 also indicates that the secondary vortices are extremely weak, illustrating that Fig.1 predicts correctly the flow geometry but misrepresents the magnitude of vorticity.

To better understand vorticity we study the stream function defined through $\mathbf{u} = \nabla \times (\phi(\mathbf{x})\hat{z}) = (\partial_y \phi(\mathbf{x}), -\partial_x \phi(\mathbf{x}))^T$, where $\mathbf{j} = en\mathbf{u}$ [see Fig. 2(b)]. This quantity has a number of useful properties. In particular, it quantifies the net integrated backflow regardless of how far from the slit the backflow occurs and the details of its spatial distribution and, as such, provides a meaningful comparison between different regimes. This quantity, shown in Fig. 2(b) on the line in the middle of the strip, $\phi_{w/2}(x) = \int_0^x j_y(\xi, w/2) d\xi$ indicates has a larger swing for the ballistic flow (blue curve) than the viscous flow (red curve), i.e. the backflow is actually somewhat stronger in the ballistic case than in the viscous case. Yet, in the absence of disorder scattering, the predicted differences between ballistic and viscous vortices are probably not strong enough to unambiguously differentiate these regimes experimentally.

To the contrary, the ballistic and viscous vortices behave very differently the presence of disorder scattering (ohmic dissipation). Namely, as illustrated in Fig. 3, a relatively weak disorder scattering is sufficient to suppress viscous vortices, while having relatively small impact on ballistic vortices, as discussed above. Usually, disorder scattering has little temperature dependence, whereas the el-el scattering is strongly temperature dependent (behaving as $\sim T^2$ in Landau Fermi-liquids). This means that the quantity γ can be tuned by varying temperature, while keeping γ_0 approximately at a constant value. As an illustration we set $\gamma_0 = 5v/w$ and vary γ (see Fig. 3(a)). We see that this dissipation value is enough to fully suppress viscous backflow (red line), while reducing the ballistic backflow (blue line) only by ~ 5 times. The property of ballistic vortices to be more resilient than viscous vortices in the presence of ohmic dissipation suggests a simple and direct diagnostic allowing to discriminate the two regimes in experiment.

It is also instructive to consider how ballistic and viscous vortices, which have approximately equal intensity in the absence of ohmic dissipation, are suppressed as the disorder scattering rate γ_0 increases, see Fig. 3 (b) and (c). In both cases we observe a transition to the ohmic

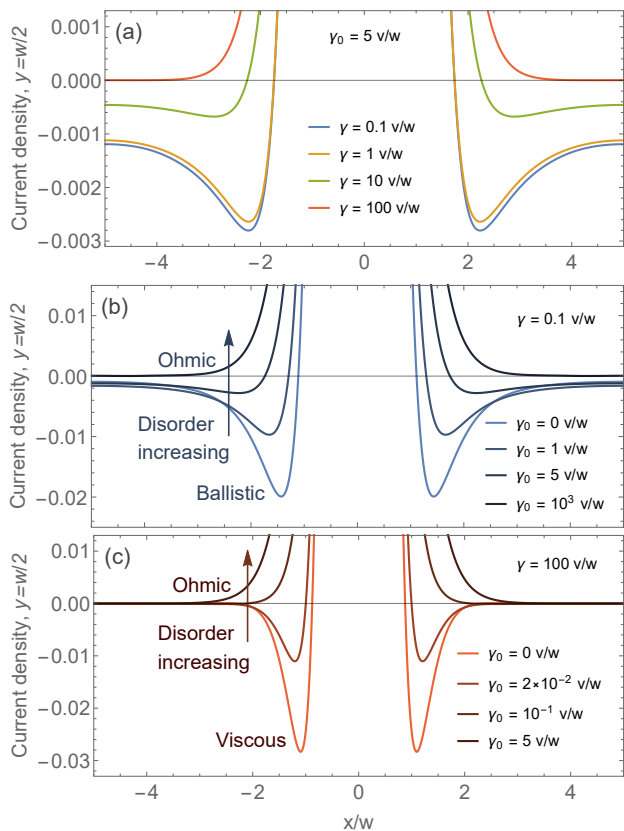


FIG. 3. Suppression of current backflow and vorticity by ohmic dissipation in different regimes. (a) Current in the middle of the strip at a fixed disorder scattering rate $\gamma_0 = 5 v/w$ and varying γ . The backflow and vorticity survive in the ballistic regime but are completely suppressed in the viscous regime. (b),(c) Weakening of the backflow upon increasing ohmic scattering in the ballistic and viscous regimes (realized at $\gamma = 0.1 v/w$ and $\gamma = 100 v/w$, respectively). Ballistic backflow is weakened roughly 2 times for $\gamma_0 = 1 v/w$, and totally suppressed for $\gamma_0 = 10^3 v/w$. Viscous backflow is considerably more fragile, being weakened roughly 2 times for $\gamma_0 = 2 \times 10^{-2} v/w$ and completely suppressed for $\gamma_0 = 5 v/w$.

flow regime that shows no backflow. Yet, the characteristic values of γ_0 above which the flow become effectively Ohmic are very different for the two cases. Vortices in ballistic regime are quite robust in the presence of ohmic dissipation and can endure disorder scattering as high as $\gamma_0 = 10^3 v/w$. For example, dissipation as small as $\gamma_0 = 2 \times 10^{-2} v/w$ results in a loss of the second (Moffatt) vortex and weakens the backflow amplitude 2 times, while for the ballistic case a similar reduction of the backflow happens for $\gamma_0 = 1 v/w$. These values are in a good agreement with the simple estimations given above in Eq.(3).

As demonstrated above, vorticity of a current flowing in a restricted geometry is a salient feature arising due to the nonlocal k -dependent conductivity that describes the current-field relation. As such, it is expected to be present and take similar values in the ballistic and viscous transport regimes. We expect the qualitative behavior found in the strip geometry — similar intensity for vorticity in the ballistic regime and in the viscous regime, the resilience of ballistic vortices in the presence of ohmic dissipation and the comparatively more fragile behavior of viscous vortices — to hold in any realistic geometry. The strikingly different dependence of vortex flows on el-el scattering and ohmic dissipation is an observable signature that can be used to discriminate the origin of vorticity in electron fluids.

Acknowledgments. We thank M. Davydova, G. Falkovich and E. Zeldov for inspiring discussions. This work was supported by the Science and Technology Center for Integrated Quantum Materials, NSF Grant No. DMR1231319; Army Research Office Grant W911NF-18-1-0116; and Bose Foundation Research fellowship.

-
- [1] A. Tomadin, G. Vignale, M. Polini, A Corbino disk viscometer for 2D quantum electron liquids Phys. Rev. Lett. 113, 235901 (2014)
- [2] A. Principi, G. Vignale, M. Carrega, M. Polini, Bulk and shear viscosities of the two-dimensional electron liquid in a doped graphene sheet Phys. Rev. B 93, 125410 (2016)
- [3] M. Qi, A. Lucas, Distinguishing viscous, ballistic, and diffusive current flows in anisotropic metals, Phys. Rev. B 104 (19), 195106 (2021)
- [4] C. Q. Cook, A. Lucas, Viscometry of electron fluids from symmetry, Phys. Rev. Lett. 127 (17), 176603 (2021)
- [5] D. Valentinis, J. Zaanen, D. van der Marel Propagation of shear stress in strongly interacting metallic Fermi liquids enhances transmission of terahertz radiation Sci. Rep. 11, 7105 (2021)
- [6] D. Valentinis, Optical signatures of shear collective modes in strongly interacting Fermi liquids Phys. Rev. Research 3, 023076 (2021)
- [7] J. Y. Khoo, P.-Y. Chang, F. Pientka, I. Sodemann Quantum paracrystalline shear modes of the electron liquid Phys. Rev. B 102 085437 (2020)
- [8] J. Y. Khoo, F. Pientka, I. Sodemann The universal shear conductivity of Fermi liquids and spinon Fermi surface states and its detection via spin qubit noise magnetometry New J. Phys. 23 113009 (2021)
- [9] L. Levitov, G. Falkovich, Electron viscosity, current vortices and negative nonlocal resistance in graphene. Nat. Phys. 12, 672 (2016).
- [10] D. A. Bandurin, I. Torre, R. Krishna Kumar, M. Ben Shalom, A. Tomadin, A. Principi, G. H. Auton, E. Khestanova, K. S. Novoselov, I. V. Grigorieva, L. A. Ponomarenko, A. K. Geim, M. Polini, Negative local resistance caused by viscous electron backflow in graphene Science Vol 351, Issue 6277, pp. 1055-1058 (2016)

- [11] F. M. D. Pellegrino, I. Torre, A. K. Geim, M. Polini, Electron hydrodynamics dilemma: Whirlpools or no whirlpools, *Phys. Rev. B* 94, 155414 (2016).
- [12] A. Lucas, K. C. Fong Hydrodynamics of electrons in graphene 2018 *J. Phys.: Condens. Matter* 30 053001
- [13] J. A. Sulpizio, L. Ella, A. Rozen, J. Birkbeck, D. J. Perello, D. Dutta, M. Ben-Shalom, T. Taniguchi, K. Watanabe, T. Holder, R. Queiroz, A. Principi, A. Stern, T. Scaffidi, A. K. Geim, S. Ilani Visualizing Poiseuille flow of hydrodynamic electrons *Nature* 576, 75-79 (2019)
- [14] M. J. H. Ku, T. X. Zhou, Q. Li, Y. J. Shin, J. K. Shi, C. Burch, L. E. Anderson, A. T. Pierce, Y. Xie, A. Hamo, U. Vool, H. Zhang, F. Casola, T. Taniguchi, K. Watanabe, M. M. Fogler, P. Kim, A. Yacoby, R. L. Walsworth Imaging viscous flow of the Dirac fluid in graphene *Nature* 583, 537-541 (2020)
- [15] B. A. Braem, F. M. D. Pellegrino, A. Principi, M. R'osli, C. Gold, S. Hennel, J. V. Koski, M. Berl, W. Dietsche, W. Wegscheider, M. Polini, T. Ihn, and K. Ensslin Scanning gate microscopy in a viscous electron fluid *Phys. Rev. B* 98, 241304(R) – Published 21 December 2018
- [16] U. Vool, A. Hamo, G. Varnavides, Y. Wang, T. X. Zhou, N. Kumar, Y. Dovzhenko, Z. Qiu, C. A. C. Garcia, A. T. Pierce, J. Gooth, P. Anikeeva, C. Felser, P. Narang, A. Yacoby Imaging phonon-mediated hydrodynamic flow in WTe₂ *Nature Physics* 17, 1216-1220 (2021)
- [17] H. Guo, E. Ilseven, G. Falkovich, L. Levitov, Higher-than-ballistic conduction of viscous electron flows. *Proc. Natl Acad. Sci. USA* 114, 3068-3073 (2017).
- [18] P. Ledwith, H. Guo, A. Shytov, L. Levitov Tomographic Dynamics and Scale-Dependent Viscosity in 2D Electron Systems, *Phys. Rev. Lett.* 123, 116601 (2019)
- [19] R. Krishna Kumar, D. A. Bandurin, F. M. D. Pellegrino, Y. Cao, A. Principi, H. Guo, G. H. Auton, M. Ben Shalom, L. A. Ponomarenko, G. Falkovich, K. Watanabe, T. Taniguchi, I. V. Grigorieva, L. S. Levitov, M. Polini, and A. K. Geim, Superballistic flow of viscous electron fluid through graphene constrictions, *Nat. Phys.* 13, 1182 (2017).
- [20] H. K. Moffatt, Viscous and resistive eddies near a sharp corner, *J. Fluid Mech.* 18 1-18 (1964)
- [21] M. Semenyakin, G. Falkovich Alternating currents and shear waves in viscous electronics *Phys. Rev. B.* 97, 8, 085127 (2018)